Environmental Science Nano

ROYAL SOCIETY OF CHEMISTRY

PAPER

View Article Online
View Journal | View Issue

Cite this: *Environ. Sci.: Nano*, 2025, **12**, 850

Interfacial adsorption and dynamics of fluorotelomers with soil minerals – mechanistic insights†

Narasimhan Loganathan, Libby Ashby, Christina E. Schumm and Angela K. Wilson *

Following the global regulation of legacy PFAS molecules, fluorotelomer molecules have been widely employed as replacements to PFOS in aqueous film-forming foam (AFFF) and PFOA in other products. Recent field studies indicate that fluorotelomer molecules are increasingly identified in environmental settings including groundwater, soil and sediments. Consequently, gaining a comprehensive understanding of the fate and transport of fluorotelomers in soils and sedimentary environments is vital. In this study, the behavior of two different fluorotelomers, 6 : 2 FTS and 6 : 2 FTC, in three common soil minerals (kaolinite, montmorillonite and illite) having quite different interfacial properties are reported using molecular dynamics simulations. The interfacial adsorption and dynamical characteristics of 6 : 2 FTS and 6 : 2 FTC vary substantially between the three minerals. Irrespective of the mineral composition, 6 : 2 FTS exhibits surface complexation while 6 : 2 FTC coordinates only with neutral and low charged clay minerals. In addition, the fundamental interactions that dictate the adsorption, interfacial structure of 6 : 2 FTS and 6 : 2 FTC are completely different for the three minerals. The large, aggregated clusters of 6 : 2 FTS at the surface experienced greater stability for longer periods of time and restricted mobility than 6 : 2 FTC for all three clay minerals. Importantly, the current study provides cluster size dependent diffusion behavior of surface adsorbed fluorotelomer molecules in each clay mineral. Such detailed mechanistic insights are necessary to understand the environmental footprint of fluorotelomers around contaminated sites.

Received 23rd May 2024,
Accepted 7th November 2024

DOI: 10.1039/d4en00465e

rsc.li/es-nano

Environmental significance

The use of fluorotelomers as replacements for legacy PFAS molecules in fire-fighting foam and other products has resulted in their footprint in the environment including in soils and sediments. This study provides detailed insights into the influence of three distinct soil minerals that vary significantly in their interfacial properties in determining the fate and transport of fluorotelomers in nano- and meso-confined pores. The current study identifies critical interactions that dictate the sorption behavior of fluorotelomers in soils and how these interactions vary with mineralogical structure and composition. Such fundamental knowledge is vital to address growing concerns about the environmental impact of fluorotelomers and provide insight into the development of targeted site-specific remediation strategies.

Introduction

The ubiquitous presence of per- and polyfluoroalkyl substances (PFAS) in environmental settings results from their widespread use in commercial, industrial and domestic applications for more than 50 years. The unique amalgamation of hydrophilic and hydrophobic character of most PFAS imparts them with extreme stability towards degradation (thermal, chemical and biological).[1,2] At the same time, toxicological studies have provided substantial evidence correlating PFAS exposure to human health impacts including cancer, thyroid, renal disease, developmental and reproductive disorders.[2–4] Consequently, legacy PFAS molecules, namely perfluorooctanoic acid (PFOA) and perfluorooctane sulfonic acid (PFOS), have been banned in the United States and in many other countries.[5] Meanwhile, substantial effort has been directed toward understanding the impact of legacy PFAS molecules on the environment and human health over the last decade.[6–11] Following the ban on legacy PFAS, there has been a sharp increase in the development of fluorotelomer-based products because of their ability to exhibit similar amphiphilic properties. For instance, fluorotelomer (FT) molecules which are a part of

Department of Chemistry and the MSU Center for PFAS Research, Michigan State University, East Lansing, Michigan 48824, USA. E-mail: akwilson@msu.edu

† Electronic supplementary information (ESI) available. See DOI: https://doi.org/10.1039/d4en00465e

the polyfluoroalkyl family (hydrophobic carbon backbone having F and H atoms) have been substituents for PFOS in aqueous film forming foam (AFFF) for nearly two decades.[12] Subsequently, an increasing number of studies report the presence of *n*:2 fluorotelomer sulfonates (FTS) in soils, sediments, and ground and surface waters.[13–18] But recent studies on biotoxicity of FTS indicate that their exposure may impact fetal development, lipid metabolism and accumulation, and, increase cardiovascular symptoms in humans and animals[19–23] (it should be noted that '*n*' in *n*:2 FTS represents the number of carbon atoms saturated with fluorine while '2' represents the number of non-fluorinated carbon atoms).

To provide examples of the presence of FTS in the environment, Dauchy *et al.*[24] examined 44 soil samples for PFAS contamination and indicated that the 6:2 FTS is one of the three molecules that is predominantly present in surface soils. Similarly, recent studies by Adamson *et al.*[25] showed elevated levels of 6:2 FTS in water and soil samples near contaminated sites. Importantly, in an examination of contaminated AFFF sites, Liu *et al.*[12] identified a higher concentration of *n*:2 FTS than perfluoroalkyl sulfonic acids (PFSA) in both soil and groundwater samples of contaminated sites. Furthermore, Liu's study emphasized that the sorption of FTS is very site-specific and is largely observed within 3 meters of the ground surface. In addition, Hubert *et al.*[16] demonstrated a weaker correlation between the soil organic matter and the adsorption capacity of 6:2 FTS than with PFOS in soil samples from AFFF contaminated sites. On the other hand, Sorengard *et al.*[14] showed that the adsorption of FT's to the mineral phases are significantly dependent on their terminal functionalities. Furthermore, in Sorengard's study, increasing adsorption of FT's with higher clay content in the soil samples (with higher illite fraction) treated with colloidal activated carbon was reported. Similarly, Nguyen *et al.*[15,26] showed that the high sorption of 6:2 FTS when compared to PFOS at the surfaces of soil minerals could be attributed to the presence of non-fluorinated carbon atoms. In addition, their studies suggested that the sorption of long chain FTS occurs at the surfaces of uncharged mineral phases and further emphasized that the sorption properties of FT's are substantially influenced by different properties of soils such as surface charge, clay content and organic matter. Meanwhile, the Barzen-Hanson *et al.*[13] investigation on a smectite rich soil sample demonstrated that the adsorption of 6:2 FTS potentially could be due to the hydrophobic interaction with the quasi-hydrophobic sites on the charged mineral surfaces. In contrast, recent studies indicated that smectites show higher adsorption capacity than neutral clays.[27]

However, much of the current understanding of 6:2 FTS is limited – gained from obtaining macroscopic distribution coefficients in soil samples. Although, the aforementioned studies imply the adsorption of 6:2 FTS at the surfaces of soil minerals with varying structural composition and surface charge characteristics, the critical factors that dictate their sorption properties such as interfacial structure, coordinated environments and dynamics of 6:2 FTS at those mineral surfaces are poorly understood. For instance, 6:2 FTS adsorption in soil minerals are typically attributed to many types of interactions such as electrostatics, hydrophobic, surface complexation, and cation bridging mechanism.[17,28] However, due to the distinct structural characteristics of minerals, the contribution of these interactions varies drastically between minerals as shown in previous experimental studies.[13,16] Even studies that have addressed such insights have centered on legacy and new age PFAS molecules.[10,29,30] To our knowledge, such adequate information is not available for 6:2 FTS and other fluorotelomers in different soil minerals, which is a prerequisite to understand their increasing distribution in soils and sediments.

At the same time, although 6:2 fluorotelomer carboxylates (FTC) are not dominantly present in soil samples, they represent some of the important transformation products during the biotransformation of amide-based PFAS and fluorotelomer alcohols (FTOH) in soils.[31–33] For instance, Ruan *et al.*[33] showed that 6:2 FTC is one of the transient acids during the transformation of 6:2 fluorotelomer iodide. Similarly, experimental studies by Zhao *et al.*[34] have shown that 6:2 FTC is one of the biodegradation products of 6:2 FTOH in sedimentary samples. Importantly, Zhang *et al.*[31] indicated that the concentration of 6:2 FTC is higher in plants than in soils. Most recently, in an examination of the photochemical transformation of FT based esters, Bugsel *et al.*[35] demonstrated the large formation of 6:2 FTC at different soil mineral surfaces. Because of the transient characteristics of 6:2 FTC, it is very difficult to assess the behavior of 6:2 FTC in soils. Thus, a critical evaluation of 6:2 FTC with common soil mineral interfaces would enable a much better comprehension of their short-lived nature at relevant environmental conditions.

The current study is one of the first investigations to critically evaluate the adsorption behavior of 6:2 FTS and 6:2 FTC in three different soil minerals, namely kaolinite, illite and montmorillonite (smectite) at relevant thermodynamic conditions. The choice of these minerals was based on experimental studies of 6:2 FTS which suggested its adsorption on neutral, illitic and smectitic surfaces at different contaminated sites.[15,16,36] Moreover, in prior studies, these three clay minerals exhibited distinct structural and layer charge distributions which resulted in completely different interfacial adsorption properties with organic and inorganic species.[29,37–43]

The main objective of the study is to provide comprehensive fundamental insight into the underlying interactions and structural factors that dictate the adsorption and dynamic characteristics of sulfonated and carboxylated fluorotelomers in three geologically relevant clay minerals on a fundamental molecular level scale. Such information's are critical to elucidate the adsorption characteristics of fluorotelomers in near- and sub-surface regions.

Simulation methods

The three minerals (namely, kaolinite, montmorillonite and illite) investigated in this study represent important mineralogical components in near-surface environments. Kaolinite belongs to 1 : 1 layered minerals where a layer of Si tetrahedra (T) is associated with Al octahedra (O). Due to the absence of isomorphic substitutions of structural atoms, kaolinite represents a neutral mineral but has both hydrophobic and hydrophilic (presence of hydroxyl groups at the 'O' side) sides exposed to bulk solutions. On the other hand, both montmorillonite and illite represent 2 : 1 layered minerals, where a layer of 'O' is sandwiched between two 'T' layers. Unlike kaolinite, these two minerals develop negative layer charges due to the isomorphic substitution of Mg^{2+}/Al^{3+} in the 'O' layer and Al^{3+}/Si^{4+} in the 'T' layer. The isomorphic substitutions in montmorillonite are located both in the 'O' (predominant) and 'T' layers and possess low structural charge. In contrast, illite, a highly charged clay mineral has all of the isomorphic substitutions exclusively in the 'T' layers. The structural composition of kaolinite used in this study is $Al_4Si_4O_{10}(OH)_8$ and is based on the optimized structure from Cygan *et al.*[44] The montmorillonite model used in this study possesses a layer charge of $-0.75|e|$ per unit cell and follows the structural composition of $M_{0.75}(Si_{7.75}Al_{0.25})(Al_{3.5}Mg_{0.5})O_{20}(OH)_4$ and has been widely employed in the examination of organic and inorganic species under natural conditions.[42,45] The illitic model has a structural formulae of $M_{1.6}(Si_{6.4}Al_{1.6})Al_4O_{20}(OH)_4$ with a layer charge of $-1.6|e|$ per unit cell.[10] It should be emphasized that the distribution of isomorphic substitutions in montmorillonite and illite were carried out in accordance with Loewenstein's rule.[46] The net negative layer charges were neutralized by the presence of the metal cations at the basal surfaces of both montmorillonite and illite. Further details about these three clay mineral models are provided in a prior study.[10] Importantly, all these three clay mineral models have been examined extensively and have shown good agreement with experimental data on the adsorption of organic and inorganic species in both nano- and meso-confined pores.[37–39,47–50]

Each of the three clay minerals were cleaved along the crystallographic (001) plane at the middle of the interlayer region to construct the external basal surface. More details about the cleavage and the resulting structural details have been discussed in our prior studies and hence provided in the ESI.†[10,29] The cleaved surfaces were kept far from each other with a total distance of ~130–135 Å between the surfaces, irrespective of the clay mineral. Such large separation between the layers effectively eliminates any influence of one surface over the other. In order to maintain a similar surface area, all three mineral surfaces were constructed with a lateral dimension of ~4500 $Å^2$. Notably, both the interlayer region and the external surface have Ca^{2+} ions to compensate for the layer charge in montmorillonite. In addition, the Ca^{2+} ions in the nanoconfined interlayer regions were hydrated with H_2O molecules; this extent of hydration is primarily based on experimental studies which show at least a partial to full monolayer of H_2O in such regions even at ambient conditions.[51] Due to non-expandable capabilities of illite, all the interlayer cations were K^+ ions while the external basal surface were exchanged for Ca^{2+} ions. All of the PFAS molecules and Ca^{2+} ions were placed ~20 Å from each other and also from the basal surface of all clay models. Importantly, the terminal functional groups of 6 : 2 FTS and 6 : 2 FTC molecules were deprotonated to mimic near-neutral pH conditions and the resulting net-negative charges were balanced by the addition of eight more Ca^{2+} ions in the water-saturated pore regions. The concentration of FT's used in this study are in ppm range which are similar to the concentrations observed near contaminated military bases and landfill sites.[52] A schematic representation of the 6 : 2 FTS, 6 : 2 FTC and simulation setup is given in the ESI† (Fig. S1a–c).

Molecular dynamics simulations were performed in the *NPT* ensemble [number of atoms (*N*), pressure (*P*) and temperature (*T*) constant] and *NVT* [number of atoms (*N*), volume (*V*) and temperature (*T*) constant] ensemble using the LAMMPS simulation package.[53] For all clay models, three-dimensional periodic boundary conditions were employed with a cutoff of 10 Å for short-range non-electrostatic interactions. The particle–particle–particle-mesh (PPPM) summation method was used to calculate the long-range electrostatics with an accuracy of $1e^{-6}$.[54] Three different interaction potentials, namely CLAYFF, SPC and GAFF2, were used to compute the interatomic interactions of clay minerals, H_2O and PFAS molecules.[55–57] Meanwhile it should be emphasized that previous studies have demonstrated that the combination of these potentials has provided good agreement with experimental studies on clay minerals.[38,43,58] A Nose–Hoover thermostat and barostat were used to control the temperature and pressure during the simulation run.[59,60] The AM1-BCC charging method in the antechamber module was used to compute the partial charges for 6 : 2 FTS and 6 : 2 FTC molecules.[61] A timestep of 1 fs was used to integrate the equations of motion. All of the simulations were performed at T – 300 K and P – 1 bar for 50 ns which includes 15 ns (10 ns – equilibration and 5 ns data production) in the NPT ensemble and subsequently 35 ns (10 ns – equilibration; 25 ns – data production) in the NVT ensemble. The last 5 ns of the production run were used for further structural and dynamical analysis with the data recorded at every 10 fs. Further details about the simulation methods and analysis can be found in our previous papers.[10,29]

Results and discussion

Atomic density profiles

The ADP's of 6 : 2 FTS and 6 : 2 FTC as functions of distance normal to the basal surfaces of three clay minerals are shown in Fig. 1–3. It is evident that the interfacial adsorption behavior is distinctly different between the three clay minerals and between the PFAS molecules. For

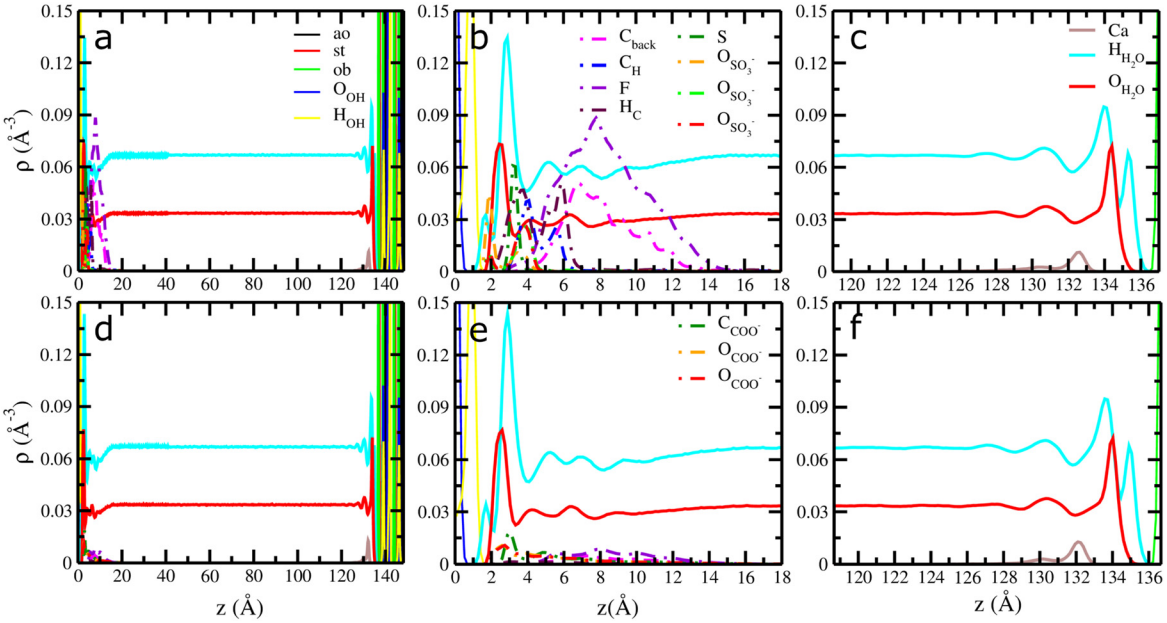

Fig. 1 Computed atomic density profiles (ADPs) of PFAS and H_2O molecules in Ca–kaolinite as a function of the distance normal to the basal hydroxyl surface. (a–c) 6 : 2 FTS (d–f) 6 : 2 FTC. H_{OH} (solid yellow) and O_{OH} (solid blue) represent the 'H' and 'O' atoms of the hydroxyl groups in kaolinite, respectively. The O_{H_2O} and H_{H_2O} are shown as solid red and cyan. Dashed lines represent the atoms of the 6 : 2 FTS/6 : 2 FTC molecules. The O_{SO_3} and S_{SO_3} represent oxygen and sulfur atoms in 6 : 2 FTS and the O_{COO} and C_{COO} represent oxygen and carboxyl carbon atoms in 6 : 2 FTS. The C_{back}, F and H_c corresponds to carbon backbone, fluorine and hydrogens in each FT's. Labels – ao, st, and ob represent surface atoms in kaolinite following the notation used in clayff.[55] The origin (z = 0) is the mean position of the basal 'O' atoms at the hydroxyl surface of kaolinite.

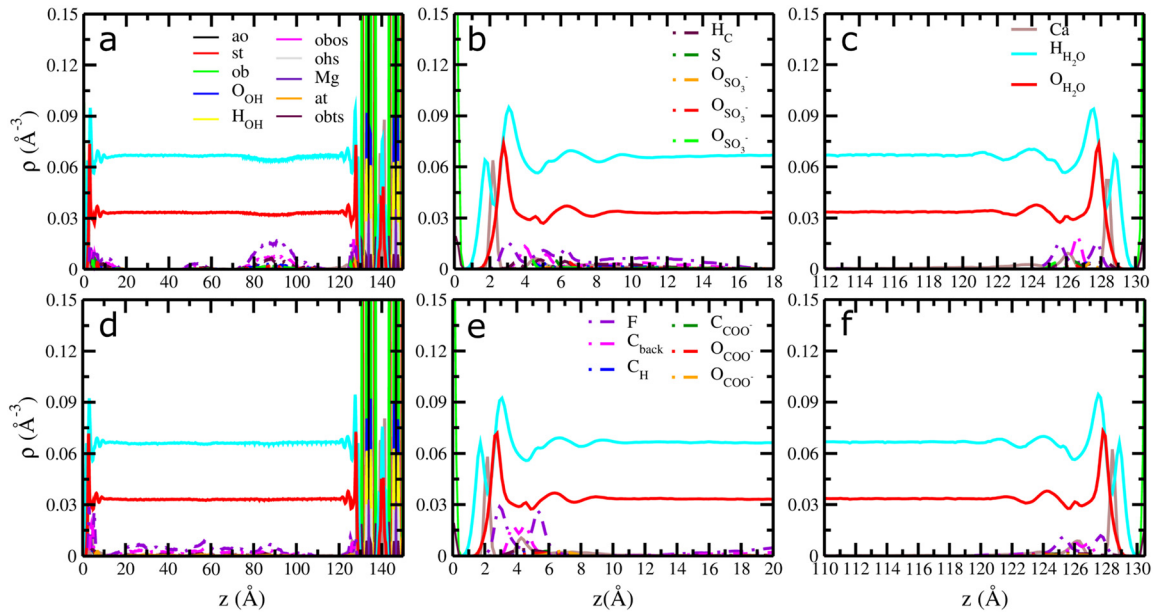

Fig. 2 Computed atomic density profiles (ADPs) of 6 : 2 FTS and 6 : 2 FTC and H_2O molecules as a function of the distance normal to the basal surface of montmorillonite. (a–c) 6 : 2 FTS (d–f) 6 : 2 FTC. The O_{H_2O} and H_{H_2O} are shown as solid red and cyan. Dashed lines represent the atoms of 6 : 2FTS/6 : 2FTC molecules. The O_{SO_3} and S_{SO_3} represent oxygen and sulfur atoms in 6 : 2 FTS and the O_{COO} and C_{COO} represent oxygen and carboxyl carbon atoms in 6 : 2 FTS. The C_{back}, F and H_c corresponds to carbon backbone, fluorine and hydrogens in each FT's. Labels – ao, at, st, ob, obts, obos and ohs represent surface atoms in montmorillonite following the notation used in clayff.[55] The origin (z = 0) is the mean position of the basal surface 'O' atoms of montmorillonite.

instance, irrespective of the terminal functionalities, the 6 : 2 FT's are exclusively adsorbed at the hydrophilic surfaces of kaolinite (Fig. 1a–f and S2a–f†) primarily due to H-bonding interactions between the terminal functional group (SO_3^-/COO^-) and the basal surface hydroxyl atoms. However, the near-surface adsorption environment varies substantially

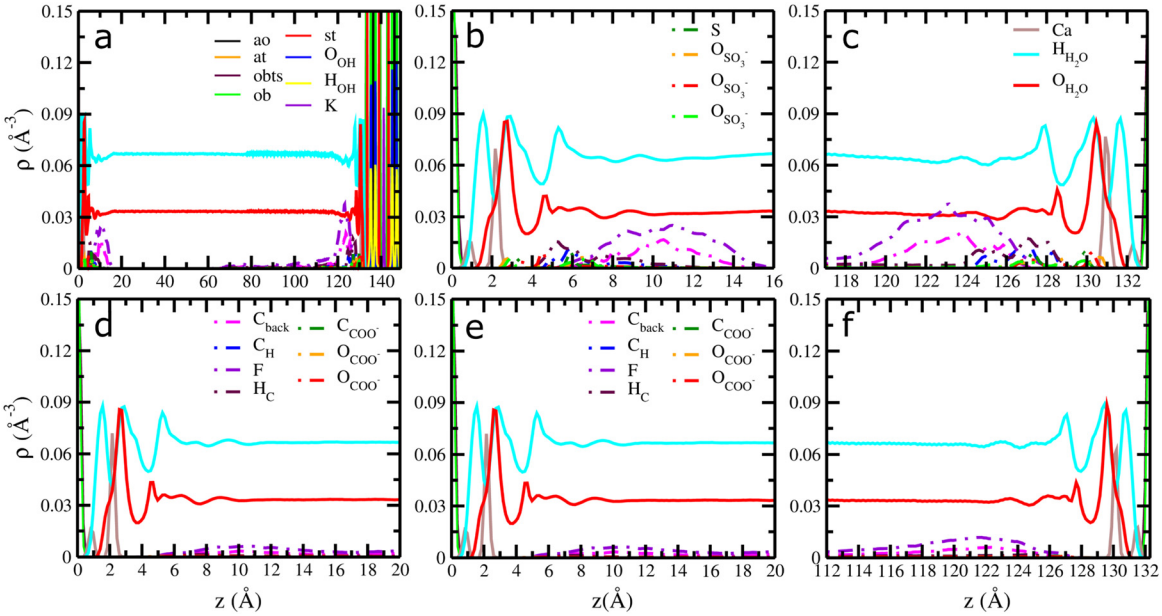

Fig. 3 Computed atomic density profiles (ADPs) of 6 : 2 FTS and 6 : 2 FTC and H_2O molecules as a function of the distance normal to the basal surface of illite. (a–c) 6 : 2 FTS (d–f) 6 : 2 FTC. The O_{H_2O} and H_{H_2O} are shown as solid red and cyan. Dashed lines represent the atoms of 6 : 2 FTS/6 : 2FTC molecules. The O_{SO_3} and S_{SO_3} represent oxygen and sulfur atoms in 6 : 2 FTS and the O_{COO} and C_{COO} represent oxygen and carboxyl carbon atoms in 6 : 2 FTS. The C_{back}, F and H_c corresponds to carbon backbone, fluorine and hydrogen in each FT's. Labels – ao, at, st, ob, and obts represent surface atoms in montmorillonite following the notation used in clayff.[55] The origin (z = 0) is the mean position of the basal surface 'O' atoms of illite.

between 6 : 2 FTS and 6 : 2 FTC. For instance, Fig. 1b and S2a† clearly demonstrates that only one 'O' atom of SO_3^- in 6 : 2 FTS exhibits dominant H-bonding interactions with the hydroxyl surface (~1.9 Å). In contrast, the remaining two 'O' atoms of SO_3^- in 6 : 2 FTS are predominantly located at z – ~3.9 Å but tend to approach the hydroxyl surface intermittently which is evident by the presence of minor peaks at z – ~1.9 Å (Fig. S2a†).

These minor peaks illustrate that those two 'O' atoms of SO_3^- groups in 6 : 2 FTS are capable of exhibiting multiple coordination with surface but such coordination does not persist for longer periods of time due to flexible substrate surface atoms which results in constant motion towards and away from the hydroxyl surface of kaolinite similar to our prior studies on PFOS.[29] The computed orientation of SO_3^- groups with respect to the surface normal of kaolinite corroborates the interfacial adsorption environment herein with a dominant non-perpendicular orientation (θ_{SO_3} – ~111°) along with a small distribution at θ_{SO_3} – ~152° (Fig. S5a†). In contrast, both the 'O' atoms of COO^- groups in 6 : 2 FTC exhibit coordination with the hydroxyl surface of kaolinite which is evident by similar peak intensities at z – ~2.6 Å. Consequently, the computed orientation of surface adsorbed COO^- groups in 6 : 2 FTC exhibits two peaks at θ_{COO} – ~117° and ~163°. The broad distribution of COO^- groups is primarily due to the rocking motion towards and away from the hydroxyl surface of kaolinite (Fig. S5b†). Notably, the interfacial adsorption structure of 6 : 2 FTC is very similar to earlier studies on PFOA in kaolinite.[29]

However, for montmorillonite, it is evident from Fig. 2a–f and S3a–f† that the adsorption of 6 : 2 FTS and 6 : 2 FTC is primarily due to the hydrophobic interactions between the PFAS molecules and the hydrophobic regions on the basal surfaces of montmorillonite. The presence of 'F' peaks and lack of peaks for 'O' atoms of SO_3^-/COO^- near the basal surface corroborates the proposed surface complexation of both fluorotelomers. Furthermore, the computed orientation of θ_{SCterm} – ~86° for 6 : 2 FTS indicates that the surface adsorbed molecules are nearly parallel to the basal surface of montmorillonite (Fig. S5c†). Similarly, the 6 : 2 FTC molecules are oriented predominantly at ~90° which indicates that the surface adsorbed 6 : 2 FTC are parallel to the basal surface (Fig. S5d†). Importantly, unlike kaolinite, the ADP's show both surface adsorbed PFAS and solution phase PFAS molecules in montmorillonite, irrespective of the terminal functionalities. However, Fig. 2a illustrates that the 6 : 2 FTS molecules are adsorbed in distinct regions of the solution phase while the 6 : 2 FTC molecules are largely dispersed across the whole solution region (Fig. 2d). Apparently, the peak distances of 'F' atoms of 6 : 2 FTC near the surface is similar to the distances reported in previous studies on GenX in montmorillonite.[10] At the same time, the APDs of illite (Fig. 3a–c and S4a–f†) clearly demonstrated that the 6 : 2 FTS are predominantly adsorbed near the basal surfaces, in complete contrast to 6 : 2 FTC which is exclusively present in the solution phase (Fig. 3d–f).

It is evident from Fig. 3b and c, that the adsorption of 6 : 2 FTS is dominated by two 'O' atoms of SO_3^- at the basal surface (z – ~2.8 Å) of illite. The surface complexation of 6 : 2 FTS is further validated by computing their orientation (θ_{SO_3} – ~162°) with respect to surface normal (Fig. S5e†). In contrast, no surface complexation of 6 : 2 FTC was observed at any simulated times. At the same time, it should be noted that the reported density profiles of Ca^{2+} ions and H_2O are not influenced by the presence of surface coordination and are very similar to the interfacial properties reported in previous studies on PFAS with minerals and hence discussed in the ESI.†[10,29]

Interfacial structure and coordination

The interfacial adsorption structure and coordination environment of both FT's at the basal surfaces of three minerals are substantially different (Fig. 4–6). For instance, there are two significant differences between 6 : 2 FTS and 6 : 2 FTC at the kaolinite surfaces:

(i) The running coordination number (RCN) of ~1.0 between the 'O' atoms of 6 : 2 FTS and the 'H' atoms of surface hydroxyl's (H_{kaol}) demonstrates that only the 'O' atoms of the SO_3^- group are responsible for surface adsorption (Fig. 4a). In contrast, due to the librational motion of the 'O' atoms in the COO^- groups towards and away from the surface, the RCN between 'O_{COO^-}' and H_{kaol} is ~0.5 (Fig. 4d)

(ii) It is evident from Fig. 4b that nearly 94% of the 6 : 2 FTS molecules exhibit direct coordination with the basal surface. In contrast, despite being near the surface, only ~40% of the 6 : 2 FTC molecules show direct coordination with the surface atoms, while the rest are associated with the surface adsorbed FTC molecules through hydrophobic interactions (Fig. 4e).

Moreover, both FT molecules demonstrate aggregated clusters at the hydroxyl surface of kaolinite, however, the size of the aggregated clusters varies depending upon their terminal functionalities. Four different stable aggregated clusters are observed for 6 : 2 FTS which includes a hexamer (6), a tetramer (3), two dimers (2) and two monomers (1) and the values in the parentheses represent the average number of molecules directly coordinated to the surface from each cluster (Fig. 4c and S7a†). On the other hand, 6 : 2 FTC aggregated clusters at the basal surface of kaolinite includes an octamer (3), a pentamer (2) and three monomers (2) as shown in Fig. 4f. However, based on the direct coordination's with the surface it is evident that the aggregated clusters of 6 : 2 FTS are highly stable than 6 : 2 FTC at the basal surface of kaolinite during the whole production run which is primarily due to their direct coordination (Fig. S7a and b†).

In montmorillonite, Fig. 5a clearly indicates a significant coordination between Ca^{2+} ions and surface adsorbed 6 : 2 FTS molecules with an RCN of ~0.3. Fig. 5b depicts that only 25% of the FTS molecules exhibit direct coordination with the basal surface of montmorillonite while the rest are predominantly in solution phase forming different clusters (more details about solution phase clusters will be discussed in the following section). It is evident from Fig. 5c that the surface adsorption is characterized by a dimer and a monomer (1). The surface adsorbed 6 : 2 FTS molecules in montmorillonite are stabilized by two different types of complexations: (i) interactions of carbon backbone with the hydrophobic regions of montmorillonite; (ii) electrostatic

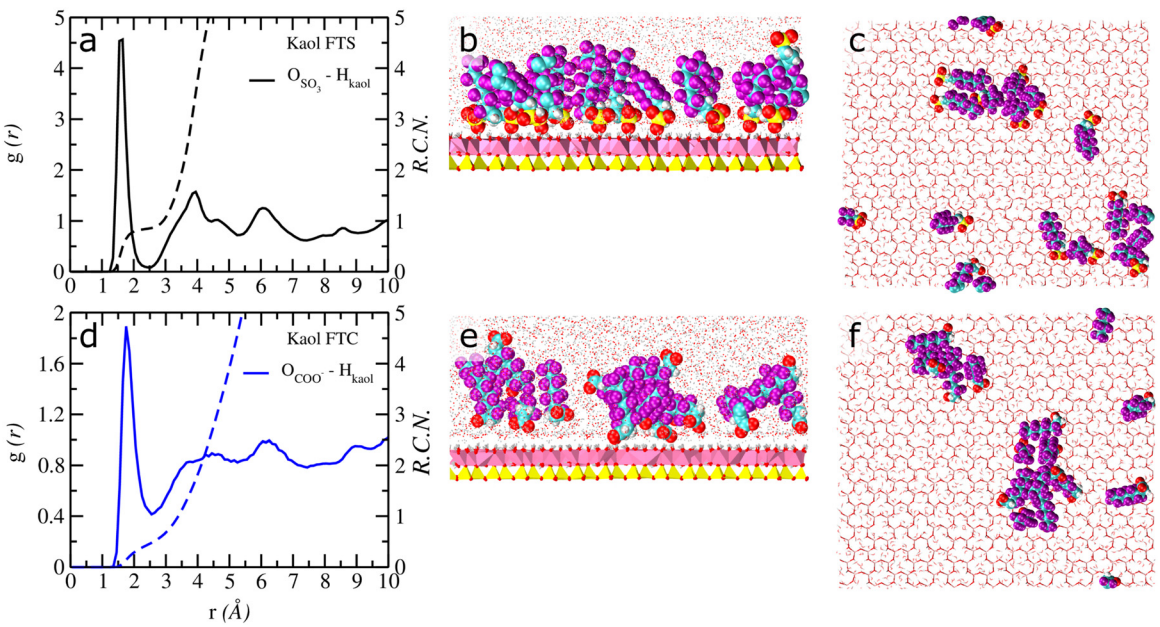

Fig. 4 Radial distribution functions (solid lines) and corresponding running coordination numbers (RCNs-dashed lines) between (a) 6 : 2 FTS and (d) 6 : 2 FTC with the basal surface hydroxyl groups in kaolinite. Pictorial representations of (b and c) surface adsorbed 6 : 2 FTS and (e and f) 6 : 2 FTC and their clusters at the basal hydroxyl surface of kaolinite.

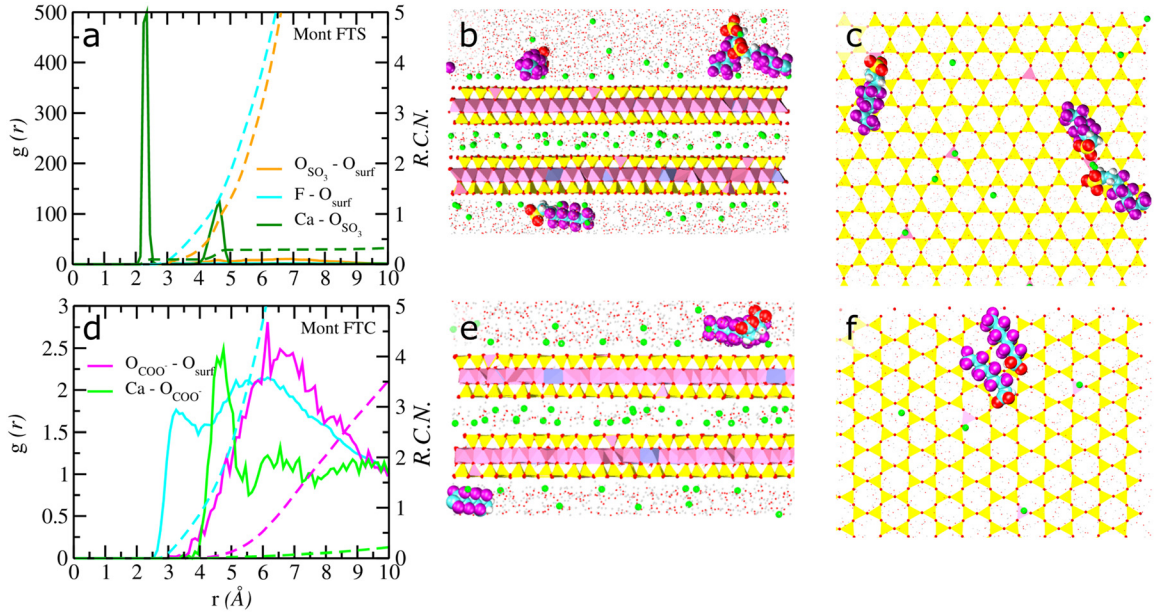

Fig. 5 Radial distribution functions (solid lines) and corresponding running coordination numbers (RCNs-dashed lines) between (a) 6 : 2 FTS and (d) 6 : 2 FTC with the basal surface adsorbed Ca^{2+} ions and 'O' atoms of montmorillonite. Pictorial representations of (b and c) surface adsorbed 6 : 2 FTS and (e and f) 6 : 2 FTC and their clusters at the basal surface of montmorillonite.

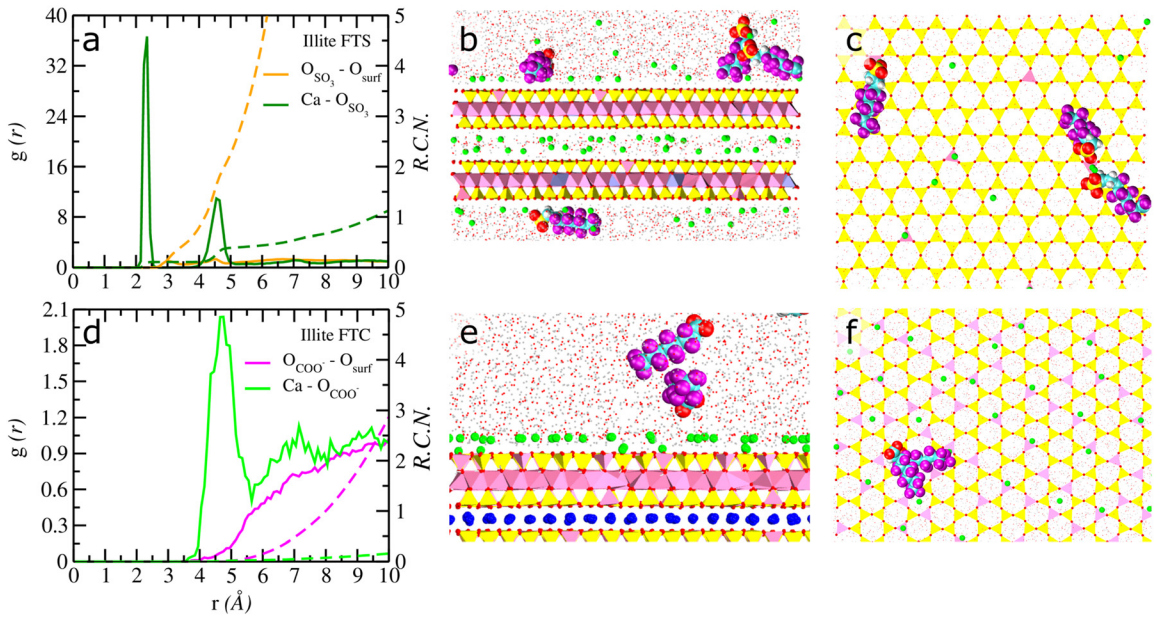

Fig. 6 Radial distribution functions (solid lines) and corresponding running coordination numbers (RCNs-dashed lines) between (a) 6 : 2 FTS and (d) 6 : 2 FTC with the basal surface adsorbed Ca^{2+} ions and 'O' atoms of illite. Pictorial representations of (b and c) surface adsorbed 6 : 2 FTS and (e and f) 6 : 2 FTC and their clusters at the basal surface of illite.

interactions between the 6 : 2 FTS with basal surface adsorbed Ca^{2+} ions. For instance, Fig. S8† clearly illustrates the coordination between the 'O' atoms of SO_3^- groups (surface adsorbed) and two different Ca^{2+} ions near the basal surface of montmorillonite. Notably, the 'O' atoms are coordinated to the Ca^{2+} ions that are adsorbed directly on top of the substituted Al tetrahedra while the other Ca^{2+} is in the diffuse region. Importantly, the presence of Ca^{2+} ion bridges between the surface adsorbed 6 : 2 FTS molecules in montmorillonite makes them highly localized and stable for longer periods of time (Fig. S8†). In contrast, it is apparent from Fig. 5d that the Ca^{2+} ions do not play a role in the coordination of 6 : 2 FTC at the basal surface of montmorillonite. The adsorption is characterized exclusively by the hydrophobic interaction between the 6 : 2 FTC molecules and the hydrophobic regions of montmorillonite

(Fig. 5e). Furthermore, the surface bound 6:2 FTC clusters include a monomer and a dimer, while the rest are predominantly in the solution region of montmorillonite (Fig. 5f).

The presence of well-defined peaks between the Ca^{2+} ions and the 'O' atoms of SO_3^- groups in Fig. 6a strongly suggests that the adsorption of 6:2 FTS with the basal surface of illite is mediated by the surface adsorbed Ca^{2+} ions. Unlike montmorillonite, it should be emphasized that nearly 75% of 6:2 FTS molecules are coordinated with the basal surfaces of illite (Fig. 6b). The remaining molecules exist in the bulk solution region. Furthermore, despite being adsorbed at the basal surface, it is evident from Fig. 6b that not all FTS molecules in illite exhibit coordination with the basal surface through Ca^{2+} ions. Instead, a few are coordinated to the basal surface of illite while the others are associated with the surface adsorbed 6:2 FTS molecules through hydrophobic interactions between the carbon backbone-forming aggregates. Unlike montmorillonite, the 6:2 FTS molecules are not adsorbed parallel to the basal surface but are oriented nearly perpendicular to the basal surfaces (Fig. S9a and b†). Such orientation is most likely due to the presence of a large number of Ca^{2+} ions at the basal surface (compensating for the structural charge) which substantially reduces any volumetric/accessible region for carbon backbone of 6:2 FTS to approach the surface.

The nature of surface adsorbed 6:2 FTS aggregated clusters in Fig. 6c and S7c† is composed of a tetramer (1), two trimers (1–2), four monomers (1). It should be noted that the value in the parentheses represents the average number of 6:2 FTS molecules exhibiting coordination with the surface through Ca^{2+} ions that are located at the top of the substituted Al tetrahedra (Fig. 6c). Furthermore, no Ca^{2+} ion bridges between the 6:2 FTS are observed in the simulations either at the surface or in the solution regions. The molecules in the solution region largely exist as monomers. It should be noted that the coordination environment for 6:2 FTC with Ca^{2+} ions were not observed since these molecules were completely dispersed in the solution phase and predominantly exist as monomers (Fig. 6d). Our simulations identified only one dimer near the diffuse region of the basal surface of illite that associates and disassociates at different time intervals (Fig. S9c†). Notably, the interfacial structure of Ca^{2+} and H_2O molecules at three clay surfaces is given in the ESI.†

Thus, it is evident from Fig. 4–6 that the formation of aggregated clusters strongly depends on the clay mineral composition and the nature of functionalities in the PFAS molecules. For charged mineral surfaces, the surface adsorbed FTS clusters are stablized by the both the presence of Ca^{2+} ions and hydrophobic interactions among themselves while the clusters of FTC are stable only due to hydrophobic interactions with the clay surfaces with no influence from surface adsorbed Ca^{2+} ions. However, the aggregated clusters in neutral kaolinite is largely stabilized by the strong H-bonding interactions with the surface and hydrophobic interactions between PFAS molecules, irrespective of the functional groups.

6:2 FTS – micellar type structure

It is important to emphasize that a large, aggregated cluster of 6:2 FTS molecules was observed in the bulk solution region of montmorillonite. The cluster encompasses eight 6:2 FTS molecules in a micellar-like structural arrangement (Fig. 7a). The molecules in the clusters are predominantly adsorbed with the hydrophobic carbon backbone forming the core and all of the terminal SO_3^- groups pointing towards the solution and are coordinated to the three Ca^{2+} ions. Importantly, the Ca^{2+} ions associated with the clusters act as bridges between the 6:2 FTS molecules in two different environments, namely the bidentate and tridentate configurations. A bidentate Ca^{2+} interacts with only one 'O' atom of SO_3^- groups from two different 6:2 FTS (orange circle), while the tridentate Ca^{2+} is coordinated to only one 'O' atom of SO_3^- groups from three different 6:2 FTS molecules (green circle). Furthermore, the RCN value of ~2.4 between the Ca^{2+} ions and the 'O' atoms of the SO_3^- groups belonging to the micelle clearly validates that there is a stable and sustained coordination between them for longer periods of time (Fig. 7b).

It should be emphasized here that, to our knowledge, this is one the first studies to report micellar-like aggregation for 6:2 FTS molecules with prevalent metal cations in saturated mesopores of soil minerals. However, it should be emphasized that although the formation of a micelle is reported earlier, such studies are limited to carboxylate PFAS (GenX) molecules in bulk solution.[62] In addition, the molecular level insights into detailed coordination environment of Ca^{2+} ions that acts as bridges between 6:2 FTS molecules in the bulk solution phase is reported for the first time. In contrast, the GenX micelle structure is formed due to only hydrophobic interactions with no metal cation bridges even at concentrations well above their critical

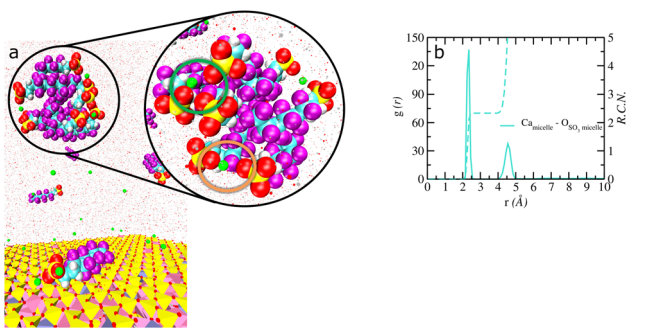

Fig. 7 Pictorial representations of the micellar type of structure of (a) 6:2 FTS in the solution phase of montmorillonite. b) Radial distribution functions (solid lines) and corresponding running coordination numbers (RCNs-dashed lines) between the solution cluster associated Ca^{2+} ions and the 'O' atoms of the 6:2 FTS belonging to the micellar type of structure in montmorillonite.

micelle concentration (CMC).[62] Notably, no such micellar type of aggregation of 6:2 FTC were observed in montmorillonite. The 6:2 FTC formed two clusters (tetramer and dimer) in the solution phase were driven by hydrophobic interactions.

Dynamical characteristics

The computed mean diffusion coefficients of both 6:2 FTS and 6:2 FTC at the mesopore regions of clay minerals demonstrate substantially different behavior between the three substrate surfaces examined. In addition, the mean diffusion varies greatly with the nature of the terminal functionalities (Table 1). For instance, irrespective of the clay mineral substrate, the mean diffusion coefficients of 6:2 FTS are substantially smaller than those of the 6:2 FTC molecules. Importantly, the diffusion coefficients of 6:2 FTS are orders of magnitude smaller than the H_2O molecules for all three clay minerals with the following sequence: kaolinite < illite < montmorillonite.

The extremely restricted mean diffusion of 6:2 FTS in kaolinite originates from the direct H-bond interactions of almost all 6:2 FTS molecules with the basal surface, despite forming large, aggregated clusters. Similarly, due to the large number of 6:2 FTS molecules interacting with the basal surface of illite (through Ca^{2+} ions), their mean diffusion is low, when compared to montmorillonite where the majority (~75%) of 6:2 FTS molecules are present in the solution phase. On the other hand, with the exception of kaolinite, the mean diffusion coefficients of 6:2 FTC are ~3–4 times smaller than for H_2O molecules in montmorillonite and illite. In contrast, the low mean diffusion coefficient of 6:2 FTC in kaolinite could be attributed to the H-bond interactions with the basal surface and the formation of large surface-bound aggregates. Nevertheless, the mean diffusion of 6:2 FTS is an order of magnitude smaller than 6:2 FTC in kaolinite which could be primarily attributed to direct interaction between the 6:2 FTS molecules with the basal surface of kaolinite. Interestingly, similar diffusion behaviors were observed for the legacy PFOS and PFOA molecules.[29]

The cluster-size dependent diffusion coefficients of surface adsorbed 6:2 FTS and 6:2 FTC is reported in Table S2† depict substantially different behavior depending upon the clay minerals. It is evident from Table S2† that the diffusion coefficients of 6:2 FTS molecules in kaolinite are very similar, irrespective of cluster size. Such diffusion characteristics are primarily attributed to their interfacial adsorption structure where nearly all 6:2 FTS molecules exhibit direct H-bonding interaction with the basal surface. In contrast, the diffusion of 6:2 FTC in kaolinite is lower for monomeric units than for clusters which is due to the ability of monomeric units to exhibit direct interaction with the basal surface of kaolinite. One of the main reasons for the clusters to show relatively high diffusion coefficients is because only a few 6:2 FTC molecules (from the cluster) exhibit direct coordination with the basal surface, while the other molecules in the clusters are coordinated through hydrophobic interactions (Fig. 4f). Similarly, with montmorillonite the surface adsorbed monomers of 6:2 FTS exhibit slower diffusion characteristics than dimers. The interfacial structure demonstrates that the surface adsorbed 6:2 FTS monomers in montmorillonite are stabilized by the 1–2 surface bound Ca^{2+} ions (located above substituted Al tetrahedra) and thus experience slow diffusion (Fig. S11a†). In contrast, the higher diffusion of 6:2 FTS dimers in contrast to that of monomers could be due to the fact that the dimers are adsorbed exclusively through hydrophobic interactions and are stabilized by Ca^{2+} ions located farther from the surface (Fig. S11b†). A similar diffusion behavior is observed for the surface adsorbed 6:2 FTC molecules with the monomer being more restricted than the dimer. However, the Ca^{2+} ions do not play a role in stabilizing the surface adsorption of 6:2 FTC (Fig. S12†). Consequently, it is evident from Table S2† that the diffusion characteristics of surface adsorbed 6:2 FTC are significantly higher than 6:2 FTS in montmorillonite.

In general, the diffusion coefficients of surface adsorbed 6:2 FTS in illite decrease with respect to increases in the cluster size. The very low diffusion characteristics of trimer may be attributed to the doubly coordinated 6:2 FTS with the surface bound Ca^{2+} ions (Fig. S13†). Due to the lack of surface adsorption of 6:2 FTC in illite, the diffusion coefficients of surface adsorbed 6:2 FTC in illite was not evaluated. Furthermore, the computed diffusion coefficient of the solution phase micellar-type structure of 6:2 FTS (4.25×10^{-10} m^2 s^{-1}) in montmorillonite is substantially slower than that of H_2O molecules which could be attributed to both the size of the micellar-type structures and the stabilization of micellar structure by Ca^{2+} ion bridges.

Table 1 Calculated diffusion coefficients (10^{-10} m^2 s^{-1}) of 6:2 FTS, 6:2 FTC and H_2O molecules in each of the three clay minerals

System	6:2 FTS	6:2 FTC	H_2O
Kaolinite	0.27	2.46	31.2
Montmorillonite	3.38	6.72	31.0
Illite	2.20	9.50	30.5

Conclusions

The current study is one of the first studies to provide a comprehensive understanding of the behavior of two fluorotelomers (6:2 FTS and 6:2 FTC) in three common soil minerals, namely kaolinite, montmorillonite and illite. Importantly, the critical interactions that govern the fate and transport of 6:2 FTS (which is one of the current alternatives used for PFOS in AFFF and is prevalent in natural settings) were determined, as well, an understanding has been gained about how these interactions vary between the neutral and charged mineral interfaces. For instance, almost all 6:2 FTS molecules are exclusively adsorbed at the basal hydroxyl surface of kaolinite through direct H-bond interactions. In

contrast, the adsorption of 6:2 FTS in montmorillonite is characterized by hydrophobic interactions between the carbon backbone and the hydrophobic region of the basal surface. Importantly, the mobility of surface adsorbed 6:2 FTS is substantially restricted by the coordination with surface adsorbed Ca^{2+} ions. Despite having high layer charge in illite, nearly ~75% of the 6:2 FTS molecules are adsorbed near the basal surface. The interfacial adsorption complexations are facilitated by the surface adsorbed Ca^{2+} ions and hydrophobic interactions between the 6:2 FTS molecules. This study also demonstrated that the surface adsorbed clusters of 6:2 FTS vary substantially between the three clay minerals. The formation of large and stable aggregated clusters in kaolinite could be responsible for their extremely low diffusion behavior.

The diffusion of 6:2 FTS in illite is relatively slower than montmorillonite which could be attributed to the greater number of molecules exhibiting surface coordination through Ca^{2+} ions. In contrast, the 6:2 FTC are dominantly present in the solution region of both charged mineral surfaces as monomers. Although, the 6:2 FTC molecules form clusters at the basal surface of kaolinite, the computed diffusion coefficients depicts that these molecules can move orders to magnitude faster than the 6:2 FTS molecules. Such interfacial adsorption and diffusion characteristics of 6:2 FTC in different minerals corroborates their transient behavior in soil environments and may elucidate why the 6:2 FTC molecules are largely found in plants than in soil.[31] Our study clearly suggest that the completely different interfacial properties of 6:2 FTS and 6:2 FTC molecules with soil minerals could be one of the reasons for FT's distribution in surface soils to be more site-specific in field studies.[12] The findings reported in this study clearly validates that the contaminated sites with high clay fraction could significantly impact the fate of PFAS depending on the site-specific mineralogical components. Since the FT's adsorption properties are significantly influenced by the common clay minerals, it is imperative to have a detailed knowledge of various constituents involved in a contaminated site and their impact on FT's when designing effective remediation strategies. However, it should be noted additional factors such as particle size, reactive edge sites and soil organic content could influence the behavior at mineral interfaces. For instance, the presence of soil organic matter at the mineral surfaces could potentially influence the formation of stable aggregates, especially when the soil organic matter is largely associated with the clay surface as shown in previous studies.[38,63,64] Based on current insights, it is evident that surface specific experiments and reactive computational methods should be employed to probe the transformation behavior of FT's at the surfaces of minerals especially near the reactive edge sites. Overall, our studies clearly show the need to have more site-specific remediation methods to address the growing concerns about fluorotelomers.

Data availability

The data supporting this article have been included as part of the ESI.†

Conflicts of interest

There are no conflicts to declare.

Acknowledgements

This material is based upon work supported by the National Science Foundation under Grant No. CHE-2107155. The authors gratefully appreciate this support. The authors also acknowledge computational resources from the National Energy Research Scientific Computing Center, which is supported by the Office of Science of the U.S. Department of Energy under ERCAP No. m1649, m4306 and the ICER computational facility at Michigan State University.

References

1 M. G. Evich, M. J. B. Davis, J. P. McCord, B. Acrey, J. A. Awkerman, D. R. U. Knappe, A. B. Lindstrom, T. F. Speth, C. Tebes-Stevens, M. J. Strynar, Z. Wang, E. J. Weber, W. M. Henderson and J. W. Washington, Per- and polyfluoroalkyl substances in the environment, *Science*, 2022, **375**, DOI: 10.1126/science.abg9065.

2 R. A. Dickman and D. S. Aga, A review of recent studies on toxicity, sequestration, and degradation of per- and polyfluoroalkyl substances (PFAS), *J. Hazard. Mater.*, 2022, **436**, 129120.

3 E. M. Sunderland, X. C. Hu, C. Dassuncao, A. K. Tokranov, C. C. Wagner and J. G. Allen, A review of the pathways of human exposure to poly- and perfluoroalkyl substances (PFASs) and present understanding of health effects, *J. Exposure Sci. Environ. Epidemiol.*, 2019, **29**, 131–147.

4 T. T. Lai, Y. Eken and A. K. Wilson, Binding of Per- and Polyfluoroalkyl Substances to the Human Pregnane X Receptor, *Environ. Sci. Technol.*, 2020, **54**, 15986–15995.

5 U.S. EPA, EPA's Per- and Polyfluoroalkyl Substances (PFAS), *Action Plan*, 2019.

6 L. Ahrens and M. Bundschuh, Fate and effects of poly- and perfluoroalkyl substances in the aquatic environment: A review, *Environ. Toxicol. Chem.*, 2014, **33**, 1921–1929.

7 E. Gagliano, M. Sgroi, P. P. Falciglia, F. G. A. Vagliasindi and P. Roccaro, Removal of poly- and perfluoroalkyl substances (PFAS) from water by adsorption: Role of PFAS chain length, effect of organic matter and challenges in adsorbent regeneration, *Water Res.*, 2020, **171**, 115381.

8 N. M. S. Almeida, S. K. Bali, D. James, C. Wang and A. K. Wilson, Binding of Per- and Polyfluoroalkyl Substances (PFAS) to the PPARγ/RXRα–DNA Complex, *J. Chem. Inf. Model.*, 2023, **63**, 7423–7443.

9 M. Smeltz, J. F. Wambaugh and B. A. Wetmore, Plasma Protein Binding Evaluations of Per- and Polyfluoroalkyl

Substances for Category-Based Toxicokinetic Assessment, *Chem. Res. Toxicol.*, 2023, **36**, 870–881.
10 C. E. Schumm, N. Loganathan and A. K. Wilson, Influence of Soil Minerals on the Adsorption, Structure, and Dynamics of GenX, *ACS ES&T Water*, 2023, **3**, 2659–2670.
11 T. R. L. Melin, P. Harell, B. Ali, N. Loganathan and A. K. Wilson, Thermochemistry of per- and polyfluoroalkyl substances, *J. Comput. Chem.*, 2023, **44**, 570–580.
12 M. Liu, G. Munoz, S. Vo Duy, S. Sauvé and J. Liu, Per- and Polyfluoroalkyl Substances in Contaminated Soil and Groundwater at Airports: A Canadian Case Study, *Environ. Sci. Technol.*, 2022, **56**, 885–895.
13 K. A. Barzen-Hanson, S. E. Davis, M. Kleber and J. A. Field, Sorption of Fluorotelomer Sulfonates, Fluorotelomer Sulfonamido Betaines, and a Fluorotelomer Sulfonamido Amine in National Foam Aqueous Film-Forming Foam to Soil, *Environ. Sci. Technol.*, 2017, **51**, 12394–12404.
14 M. Sorengard, D. B. Kleja and L. Ahrens, Stabilization of per- and polyfluoroalkyl substances (PFASs) with colloidal activated carbon (PlumeStop®) as a function of soil clay and organic matter content, *J. Environ. Manage.*, 2019, **249**, 109345.
15 T. M. H. Nguyen, J. Bräunig, K. Thompson, J. Thompson, S. Kabiri, D. A. Navarro, R. S. Kookana, C. Grimison, C. M. Barnes, C. P. Higgins, M. J. McLaughlin and J. F. Mueller, Influences of Chemical Properties, Soil Properties, and Solution pH on Soil–Water Partitioning Coefficients of Per- and Polyfluoroalkyl Substances (PFASs), *Environ. Sci. Technol.*, 2020, **54**, 15883–15892.
16 M. Hubert, H. P. H. Arp, M. C. Hansen, G. Castro, T. Meyn, A. G. Asimakopoulos and S. E. Hale, Influence of grain size, organic carbon and organic matter residue content on the sorption of per- and polyfluoroalkyl substances in aqueous film forming foam contaminated soils – Implications for remediation using soil washing, *Sci. Total Environ.*, 2023, **875**, 162668.
17 R. S. Kookana, D. A. Navarro, S. Kabiri and M. J. McLaughlin, Key properties governing sorption–desorption behaviour of poly- and perfluoroalkyl substances in saturated and unsaturated soils: a review, *Soil Res.*, 2022, **61**, 107–125.
18 B. Xu, S. Liu, J. L. Zhou, C. Zheng, J. Weifeng, B. Chen, T. Zhang and W. Qiu, PFAS and their substitutes in groundwater: Occurrence, transformation and remediation, *J. Hazard. Mater.*, 2021, **412**, 125159.
19 M. Camdzic, D. S. Aga and G. E. Atilla-Gokcumen, Cellular Interactions and Fatty Acid Transporter CD36-Mediated Uptake of Per- and Polyfluorinated Alkyl Substances (PFAS), *Chem. Res. Toxicol.*, 2022, **35**, 694–702.
20 M. E. Bohannon, A. M. Narizzano, B. A. Guigni, A. G. East and M. J. Quinn, Next-generation PFAS 6:2 fluorotelomer sulfonate reduces plaque formation in exposed white-footed mice, *Toxicol. Sci.*, 2023, **192**, 97–105.
21 M. Appel, M. Forsthuber, R. Ramos, R. Widhalm, S. Granitzer, M. Uhl, M. Hengstschläger, T. Stamm and C. Gundacker, The transplacental transfer efficiency of per- and polyfluoroalkyl substances (PFAS): a first meta-analysis, *J. Toxicol. Environ. Health, Part B*, 2022, **25**, 23–42.
22 E. Marques, M. Pfohl, W. Wei, G. Tarantola, L. Ford, O. Amaeze, J. Alesio, S. Ryu, X. Jia, H. Zhu, G. D. Bothun and A. Slitt, Replacement per- and polyfluoroalkyl substances (PFAS) are potent modulators of lipogenic and drug metabolizing gene expression signatures in primary human hepatocytes, *Toxicol. Appl. Pharmacol.*, 2022, **442**, 115991.
23 L. Wang, S. Chen, H. Hou, M. Cao, Z. Zhou, H. Cao, M. Chen, Y. Liang and Y. Wang, Early Stage Exposure of 1H,1H,2H,2H-Perfluorooctanesulfonate-Induced Cardiovascular Abnormality in Zebrafish Embryos and Larvae, *ACS ES&T Water*, 2023, **3**, 106–117.
24 X. Dauchy, V. Boiteux, A. Colin, J. Hémard, C. Bach, C. Rosin and J.-F. Munoz, Deep seepage of per- and polyfluoroalkyl substances through the soil of a firefighter training site and subsequent groundwater contamination, *Chemosphere*, 2019, **214**, 729–737.
25 D. T. Adamson, P. R. Kulkarni, A. Nickerson, C. P. Higgins, J. Field, T. Schwichtenberg, C. Newell and J. J. Kornuc, Characterization of relevant site-specific PFAS fate and transport processes at multiple AFFF sites, *Environ. Adv.*, 2022, **7**, 100167.
26 T. M. H. Nguyen, J. Bräunig, R. S. Kookana, S. L. Kaserzon, E. R. Knight, H. N. P. Vo, S. Kabiri, D. A. Navarro, C. Grimison, N. Riddell, C. P. Higgins, M. J. McLaughlin and J. F. Mueller, Assessment of Mobilization Potential of Per- and Polyfluoroalkyl Substances for Soil Remediation, *Environ. Sci. Technol.*, 2022, **56**, 10030–10041.
27 A. Ahmad, K. Tian, B. Tanyu and G. D. Foster, Effect of Clay Mineralogy on the Partition Coefficients of Perfluoroalkyl Substances, *ACS ES&T Water*, 2023, **3**, 2899–2909.
28 W. Cai, D. A. Navarro, J. Du, G. Ying, B. Yang, M. J. McLaughlin and R. S. Kookana, Increasing ionic strength and valency of cations enhance sorption through hydrophobic interactions of PFAS with soil surfaces, *Sci. Total Environ.*, 2022, **817**, 152975.
29 N. Loganathan and A. K. Wilson, Adsorption, Structure, and Dynamics of Short- and Long-Chain PFAS Molecules in Kaolinite: Molecular-Level Insights, *Environ. Sci. Technol.*, 2022, **56**, 8043–8052.
30 J. A. R. Willemsen and I. C. Bourg, Molecular dynamics simulation of the adsorption of per- and polyfluoroalkyl substances (PFASs) on smectite clay, *J. Colloid Interface Sci.*, 2021, **585**, 337–346.
31 H. Zhang, B. Wen, X. Hu, Y. Wu, L. Luo, Z. Chen and S. Zhang, Determination of fluorotelomer alcohols and their degradation products in biosolids-amended soils and plants using ultra-high performance liquid chromatography tandem mass spectrometry, *J. Chromatogr. A*, 2015, **1404**, 72–80.
32 S. Zhang, B. Szostek, P. K. McCausland, B. W. Wolstenholme, X. Lu, N. Wang and R. C. Buck, 6:2 and 8:2 fluorotelomer alcohol anaerobic biotransformation in digester sludge from a WWTP under methanogenic conditions, *Environ. Sci. Technol.*, 2013, **47**, 4227–4235.

33 T. Ruan, B. Szostek, P. W. Folsom, B. W. Wolstenholme, R. Liu, J. Liu, G. Jiang, N. Wang and R. C. Buck, Aerobic soil biotransformation of 6:2 fluorotelomer iodide, *Environ. Sci. Technol.*, 2013, **47**, 11504–11511.

34 L. Zhao, P. W. Folsom, B. W. Wolstenholme, H. Sun, N. Wang and R. C. Buck, 6:2 Fluorotelomer alcohol biotransformation in an aerobic river sediment system, *Chemosphere*, 2013, **90**, 203–209.

35 B. Bugsel, M. Schüßler, J. Zweigle, M. Schmitt and C. Zwiener, Photocatalytical transformation of fluorotelomer- and perfluorosulfonamide-based PFAS on mineral surfaces and soils in aqueous suspensions, *Sci. Total Environ.*, 2023, **894**, 164907.

36 J. Hatton, C. Holton and B. DiGuiseppi, Occurrence and behavior of per- and polyfluoroalkyl substances from aqueous film-forming foam in groundwater systems, *Remediation*, 2018, **28**, 89–99.

37 N. Loganathan and A. G. Kalinichev, Quantifying the Mechanisms of Site-Specific Ion Exchange at an Inhomogeneously Charged Surface: Case of Cs+/K+ on Hydrated Muscovite Mica, *J. Phys. Chem. C*, 2017, **121**, 7829–7836.

38 N. Loganathan, R. James Kirkpatrick and G. M. Bowers, A mechanistic exploration of natural organic matter aggregation and surface complexation in smectite mesopores, *J. Phys. Chem. A*, 2020, **124**, 9832–9843.

39 A. G. Kalinichev, N. Loganathan, B. F. N. Wakou and Z. Chen, Interaction of Ions with Hydrated Clay Surfaces: Computational Molecular Modeling for Nuclear Waste Disposal Applications, *Procedia Earth Planet. Sci.*, 2017, **17**, 566–569.

40 J. A. Greathouse, R. T. Cygan, J. T. Fredrich and G. R. Jerauld, Adsorption of Aqueous Crude Oil Components on the Basal Surfaces of Clay Minerals: Molecular Simulations Including Salinity and Temperature Effects, *J. Phys. Chem. C*, 2017, **121**, 22773–22786.

41 K. D. Papavasileiou, V. K. Michalis, L. D. Peristeras, M. Vasileiadis, A. Striolo and I. G. Economou, Molecular Dynamics Simulation of Water-Based Fracturing Fluids in Kaolinite Slit Pores, *J. Phys. Chem. C*, 2018, **122**, 17170–17183.

42 N. Loganathan, G. M. Bowers, B. F. N. Wakou, A. G. Kalinichev, R. J. Kirkpatrick and A. O. Yazaydin, Understanding methane/carbon dioxide partitioning in clay nano- and meso-pores with constant reservoir composition molecular dynamics modeling, *Phys. Chem. Chem. Phys.*, 2019, **21**, 6917–6924.

43 J. A. Greathouse, D. B. Hart, G. M. Bowers, R. J. Kirkpatrick and R. T. Cygan, Molecular Simulation of Structure and Diffusion at Smectite–Water Interfaces: Using Expanded Clay Interlayers as Model Nanopores, *J. Phys. Chem. C*, 2015, **119**, 17126–17136.

44 I. F. Vasconcelos, B. A. Bunker and R. T. Cygan, Molecular dynamics modeling of ion adsorption to the basal surfaces of kaolinite, *J. Phys. Chem. C*, 2007, **111**, 6753–6762.

45 B. F. Ngouana-Wakou and A. G. Kalinichev, Structural arrangements of isomorphic substitutions in smectites: Molecular simulation of the swelling properties, interlayer structure, and dynamics of hydrated cs-montmorillonite revisited with new clay models, *J. Phys. Chem. C*, 2014, **118**, 12758–12773.

46 W. Loewenstein, The distribution of aluminum in the tetrahedra of silicates and aluminates, *Am. Mineral.*, 1954, **39**, 92–96.

47 N. Loganathan, A. O. Yazaydin, G. M. Bowers, B. F. Ngouana-Wakou, A. G. Kalinichev and R. J. Kirkpatrick, Role of Cations in the Methane/Carbon Dioxide Partitioning in Nano- And Mesopores of Illite Using Constant Reservoir Composition Molecular Dynamics Simulation, *J. Phys. Chem. C*, 2020, **124**, 2490–2500.

48 H. T. Schaef, N. Loganathan, G. M. Bowers, R. J. Kirkpatrick, A. O. Yazaydin, S. D. Burton, D. W. Hoyt, K. S. Thanthiriwatte, D. A. Dixon, B. P. McGrail, K. M. Rosso, E. S. Ilton and J. S. Loring, Tipping Point for Expansion of Layered Aluminosilicates in Weakly Polar Solvents: Supercritical CO2, *ACS Appl. Mater. Interfaces*, 2017, **9**, 36783–36791.

49 R. Šolc, M. H. Gerzabek, H. Lischka and D. Tunega, Wettability of kaolinite (001) surfaces – Molecular dynamic study, *Geoderma*, 2011, **169**, 47–54.

50 S. Tian, V. Erastova, S. Lu, H. C. Greenwell, T. R. Underwood, H. Xue, F. Zeng, G. Chen, C. Wu and R. Zhao, Understanding Model Crude Oil Component Interactions on Kaolinite Silicate and Aluminol Surfaces: Toward Improved Understanding of Shale Oil Recovery, *Energy Fuels*, 2018, **32**, 1155–1165.

51 B. F. Ngouana-Wakou and A. G. Kalinichev, Modélisation moléculaire de l'hydratation, de la structure, et de la mobilité des ions et de l'eau dans l'espace interfoliaire et à la surface d'une argile smectitique, 2014.

52 K. Dasu, X. Xia, D. Siriwardena, T. P. Klupinski and B. Seay, Concentration profiles of per- and polyfluoroalkyl substances in major sources to the environment, *J. Environ. Manage.*, 2022, **301**, 113879.

53 S. Plimpton, Fast Parallel Algorithms for Short-Range Molecular Dynamics, *J. Comput. Phys.*, 1995, **117**, 1–19.

54 S. Plimpton, R. Pollock and M. Stevens, in *PPSC*, 1997.

55 R. T. Cygan, J.-J. Liang and A. G. Kalinichev, Molecular Models of Hydroxide, Oxyhydroxide, and Clay Phases and the Development of a General Force Field, *J. Phys. Chem. B*, 2004, **108**, 1255–1266.

56 J. Wang, R. M. Wolf, J. W. Caldwell, P. A. Kollman and D. A. Case, Development and testing of a general amber force field, *J. Comput. Chem.*, 2004, **25**, 1157–1174.

57 O. Teleman, B. Jönsson and S. Engström, A molecular dynamics simulation of a water model with intramolecular degrees of freedom, *Mol. Phys.*, 1987, **60**, 193–203.

58 N. Loganathan, A. O. Yazaydin, G. M. Bowers, A. G. Kalinichev and R. J. Kirkpatrick, Cation and Water Structure, Dynamics, and Energetics in Smectite Clays: A Molecular Dynamics Study of Ca-Hectorite, *J. Phys. Chem. C*, 2016, **120**, 12429–12439.

59 W. Shinoda, M. Shiga and M. Mikami, Rapid estimation of elastic constants by molecular dynamics simulation under

constant stress, *Phys. Rev. B: Condens. Matter Mater. Phys.*, 2004, **69**, 134103.

60 M. E. Tuckerman, J. Alejandre, R. López-Rendón, A. L. Jochim and G. J. Martyna, A Liouville-operator derived measure-preserving integrator for molecular dynamics simulations in the isothermal–isobaric ensemble, *J. Phys. A: Math. Gen.*, 2006, **39**, 5629–5651.

61 A. Jakalian, B. L. Bush, D. B. Jack and C. I. Bayly, Fast, efficient generation of high-quality atomic charges. AM1-BCC model: I. Method, *J. Comput. Chem.*, 2000, **21**, 132–146.

62 S. Kancharla, A. Choudhary, R. T. Davis, D. Dong, D. Bedrov, M. Tsianou and P. Alexandridis, GenX in water: Interactions and self-assembly, *J. Hazard. Mater.*, 2022, **428**, 128137.

63 R. Sutton and G. Sposito, Molecular simulation of humic substance-Ca-montmorillonite complexes, *Geochim. Cosmochim. Acta*, 2006, **70**, 3566–3581.

64 G. M. Bowers, D. W. Hoyt, S. D. Burton, B. O. Ferguson, T. Varga and R. J. Kirkpatrick, In Situ 13C and 23Na Magic Angle Spinning NMR Investigation of Supercritical CO2 Incorporation in Smectite–Natural Organic Matter Composites, *J. Phys. Chem. C*, 2014, **118**, 3564–3573.

